郑丽萍, 甘永德, 贾仰文, 等. 基于分层土壤的水土调控方法试验[J]. 南水北调与水利科技(中英文), 2023, 21(4): 708-730. ZHENG L P, GAN Y D, JIA Y W, et al. Experimental study on water and soil regulation method based on layered soil[J]. South-to-North Water Transfers and Water Science & Technology, 2023, 21(4): 708-730. (in Chinese)

基于分层土壤的水土调控方法试验

郑丽萍[1], 甘永德[1], 贾仰文[2], 吴玉帅[1], 刘欢[2], 袁日萍[1]

(1. 青海大学水利电力学院/黄河上游生态保护与高质量发展实验室, 西宁 810016;
2. 中国水利水电科学研究院 流域水循环模拟与调控国家重点实验室, 北京 100038)

摘要: 以土壤物理学原理为指导, 充分利用土壤基本物理性质, 提出一种通过调整土壤剖面的分层组合方式, 达到调控水土过程的技术, 命名为人工分层配土(artificially layered soil, ALS)工程。为验证人工分层配土工程在水土调控方面的作用, 开展室内积水入渗试验、植被蒸散发试验和野外干旱区土壤水分观测试验。结果表明: 室内试验中, 通过调整土壤剖面结构, 人工分层配土显著提高了土壤的入渗能力, 初始入渗速率提高 3 倍以上, 平均入渗速率提高 67.57 %, 土壤累计入渗量增加 47.14 %, 同时降低了表层土壤含水量, 减少 38.39 % 土壤的无效蒸发量; 野外试验中, 分层配土处理组土壤含水量主要储存在地表下 31~50 cm 处, 而野外原状土土壤含水量主要位于表层土壤, 且相较于原状土壤, 人工分层配土耗水量减少 13.32 %, 耗水速率降低 12.90 %。因此, 人工分层配土工程实现了水土调控的目的, 对干旱区水土资源调控和荒漠化防治具有重要的意义。

关键词: 土壤物理性质; 土壤分层; 土壤含水量; 土壤蒸发; 土壤入渗

中图分类号: TV213;S152 **文献标志码:** A **DOI:** 10.13476/j.cnki.nsbdqk.2023.0070

干旱区除降雨量较少外, 土壤蒸发和水土流失也会造成水分的无效损失, 导致水资源的短缺和土壤的退化[1-2]。植被建设是生态环境建设的重要组成部分, 植被具有拦蓄降雨、减少径流、固持土壤、防止侵蚀和改善生态环境等作用, 是生态系统物质循环和能量交换的枢纽, 也是防止生态退化的物质基础[3], 在改善生态环境等方面发挥着十分重要的作用[4]。土壤水分是植物水分利用的重要来源之一, 是生存和生长必需的营养物质, 在植物的光合作用、呼吸作用以及养分运输等生理过程中都发挥着不可替代的作用, 也是植被建设极为重要的生态限制因素[5-6]。在干旱区, 自然降水是土壤水分主要来源之一, 故探索有效的水土调控措施, 开展区域现有雨水高效利用对解决干旱区绿化具有重要科学意义。

抗旱造林整地技术是干旱半干旱地区抗旱造林的重要基础, 对树种生长、发育的影响巨大, 主要目的在于蓄水保墒。当前的整地具体包含反坡水平沟、反坡水平阶、水平阶、鱼鳞坑以及覆盖塑料地膜等[7-11], 一般通过人工或者机械的方式开展。干旱区除本身降雨量较小外, 主要由于土壤入渗能力较低和无效蒸发量较大, 当前这些整地技术无法显著提高土壤入渗能力和降低土壤无效蒸发量, 故难以达到雨水高效利用的目的。研究表明, 土壤入渗特性和蒸散发特性, 可以通过改良土壤物理性质和分层组合方式实现[12-13]。另外, 自然条件下, 由于土壤膨胀性、根系和虫孔等影响, 土壤发育大量干缩裂隙和大孔隙, 极大地影响土壤入渗过程[14]。一方面, 土壤中碎石的存在使土体内孔隙比例增大[15-17], 水流通道增多, 促进大孔隙优先流的形成, 降雨形成壤中流和入渗流的部分增多, 产流减少[18-20]; 另一方面, 碎石也会增加水流弯曲度、减小过水断面, 阻碍入渗, 周蓓蓓等[21] 研究发现碎石含量和大小决定两方面作用的优势比重。干缩裂隙和大孔隙是降

收稿日期: 2023-03-08 **修回日期:** 2023-06-29 **网络出版时间:** 2023-08-08
网络出版地址: https://link.cnki.net/urlid/13.1430.TV.20230807.1628.002
基金项目: 国家自然科学基金项目(51909129); 青海省重大科技专项(2021-SF-134)
作者简介: 郑丽萍(1997—), 女, 四川南部人, 主要从事干旱区水土调控研究。E-mail: zlp113@qhu.edu.cn
通信作者: 甘永德(1985—), 男, 青海民和人, 副教授, 博士研究生, 主要从事流域水循环模拟、干旱区水土调控和水资源规划管理研究。E-mail: bjganyd@163.com

雨期雨水进入土壤的优先流通道[22-25]，促进雨水快速下渗。沙土具有强导水性、弱持水性的特点，降雨期间可以快速入渗和储存水分，同时史文娟等[26]研究发现沙土层会抑制毛管水上升的速度，也会影响毛管水上升的高度。因此与均质土相比，沙层会将水分滞留于下层土壤中，也会显著延长上层土壤含水量达到某一程度所需的时间，从而影响表层土壤含水量，故沙土能有效抑制土壤的蒸发能力[27]，进而降低土壤无效蒸发量。

以往的研究侧重土石混合介质，夹沙层等单独对水分运动过程的影响，本研究结合土石混合介质和沙土，利用土壤分层[28]和土壤膨胀性等基本物理性质，对土壤结构进行调整，定量分析人工分层配土对入渗、土壤水分再分布和蒸散发等土壤水文过程所产生的影响，在经济环保的基础上提高土壤的下渗能力，降低土壤的无效蒸发，使土壤水分储存在较深层供植物利用，而表层土壤则维持在低含水量的状态，实现了土壤水土调控的目的，以期为干旱区生态环境治理修复提供一定的技术与理论支持。

1　人工分层配土设计

通过文献调研及前期研究基础，已开展了土壤分层组合方式、土石混合介质对入渗过程影响的相关研究，在人工分层土壤设计过程中也充分考虑了这些影响因素。因此，利用土壤分层、土石混合介质等物理性质，改变现有自然条件下的土壤分层组合方式，从而改变土壤入渗能力和蒸散发等土壤水文过程，进而达到调控水土的目的，具体改良措施如下：

针对有一定坡度（5° ~ 25°）的区域，工程内容具体包括在原始土壤表面挖沙沟，沙沟内填沙，在填完沙的沙沟上覆盖膨胀性土壤土石混合介质层，见图 1。由于新改造的土壤是在原来土壤层上人工配置了两层新的土壤层，改变了土壤原有的分层组合方式，因此命名为人工分层配土工程。

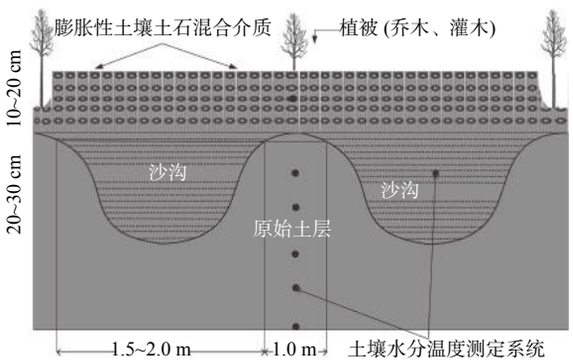

图 1　人工分层配土工程横截面

Fig. 1　Schematic diagram of cross-section of artificial layered soil engineering

土石混合介质层包括土壤和碎石（碎石粒径 1~3 cm，质量占总质量的 40 %），沙沟由沙土组成，沙沟横截面呈椭圆形，长直径为 1.5~2.0 m，短直径为 0.2~0.4 m，两个相邻沙沟形成波浪线型，沙沟之间种植植被。

2　材料与方法

2.1　室内试验

2.1.1　试验材料

供试土壤选择沙土、碎石（粒径 1~3 cm）和壤土。所有土壤经风干后过筛备用（壤土 2 mm；沙土 2 mm）。土壤采用烘干法测定土壤初始含水量、干容重和饱和含水量，采用吸管法测定土壤颗粒组成，用定水头法测定饱和导水系数，结果见表 1。碎石粒径为 1~3 cm，为建筑砂石。土石混合介质由壤土和碎石混合而得，混合比例为碎石占总质量的 40 %。试验所用水样取自室内自来水。

表 1　土壤基本物理性质

Tab. 1　Basic physical properties of soil

土壤类型	干密度/ ($g \cdot cm^{-3}$)	饱和导水系数/ ($cm \cdot min^{-1}$)	饱和含水量/ ($cm^3 \cdot cm^{-3}$)	残余含水量/ ($cm^3 \cdot cm^{-3}$)	粒径分布/%		
					>50 μm	2 ~ 50 μm	<2 μm
沙土	1.60	0.960	0.38	0.05	96.34	3.66	0
壤土	1.36	0.064	0.42	0.06	38.06	40.01	21.93

2.1.2　试验方法

试验于青海大学水利大厅实验室开展，采用垂直土柱法（土柱高 60 cm，内径 40 cm）进行。试验分为垂向一维积水入渗试验和植被耗水试验，每个试验均设置 2 个处理，分别为人工分层配土（ALS）和均质无分层土壤（non-artificially layered soil，NLS），NLS 为均质壤土。试验装置由土柱、马氏瓶、称量设备和数据采集器构成。

对于人工分层配土(ALS)处理组:土壤装填时,首先在土槽底部铺设反滤作用的砂石,厚度约为 10 cm;再在砂石的上面铺设纱布,然后按人工分层土壤分层组合方式顺序填装壤土、沙土和土石混合介质,密度分别为壤土 1.36 g/cm^3、沙土 1.60 g/cm^3、土石混合介质 1.56 g/cm^3。由于土柱直径较小,装填土壤时对沙沟进行了缩小(呈抛物线型),具体见图 2。为了确定剖面土壤水分,在土柱中心 5、15、25、35 cm 和与土柱 17.5 cm 相对应的沙土层 7.5 cm 处安装 EM50 土壤温度水分传感器,用以测定土壤 0~10 cm、31~40 cm 和沙土层 0~15 cm 深度处的土壤含水量,而土壤 11~20 cm 和 21~30 cm 处的含水量根据土柱中心 15 cm、25 cm 的土壤水分数据分别与沙土层 7.5 cm 处的水分数据加权平均确定。

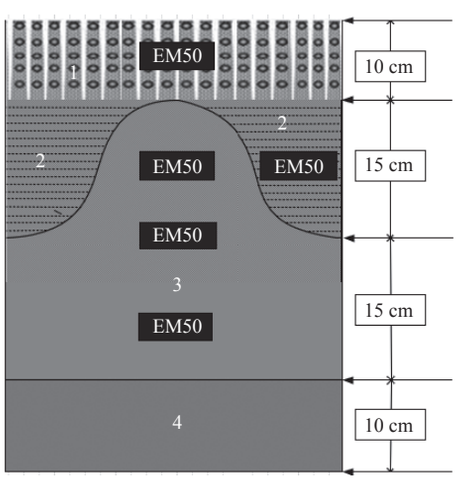

图 2　人工分层配土试验土壤剖面

Fig. 2　Schematic diagram of soil profile for artificial layered soil experiment

注:1:土石混合介质层;2:沙土层;3:壤土层;4:砂石层。

对于均质无分层土壤(NLS)处理组:土壤装填时,首先在土槽底部铺设反滤作用的砂石,厚度约为 10 cm;再在砂石的上面铺设纱布,然后按自然条件下土壤的组成方式装填壤土,壤土密度为 1.36 g/cm^3。为了测定剖面土壤含水量,在处理组的土柱中心 5、15、25、35 cm 处安装 EM50 土壤温度水分传感器,用以测定土壤 0~10 cm、11~20 cm、21~30 cm、31~40 cm 深度处的土壤含水量。

试验用马氏瓶恒压供水。在试验过程测定马氏瓶读数和土柱内积水深度,计算得到时段内土壤的累计入渗量。在试验时段内,EM50 水分传感器每隔 20 min 记录一次土壤含水量。

积水入渗试验。试验进行前,向土槽注入足够水量(土壤达到田间持水量以上,并产生大量壤中流)后静置风干后开展入渗试验。采用马式瓶供水,入渗历时控制在 90 min 左右。其间室内温度为 25 ℃左右,主要观测资料:马式瓶读数、入渗历时等。

植被耗水试验。试验填土方式和所用仪器同入渗试验。如图 1 所示,填完土后,再在原土层凸面(沙沟中间)栽种植物(吊兰 1 株),然后向土柱注入大量水分(土壤达到田间持水量以上,并产生大量壤中流)后开始试验。试验于 2018 年 8 月 5 日开始,至 2018 年 12 月 22 日结束,期间室内温度为 25 ℃左右,室内湿度为 15 %。每隔 10~20 d 灌水 1 次,采用称重法测定土壤蒸散发量(精度 0.1 g),测定频率为 1 次/周,灌水前后加测。

2.2　野外试验

2.2.1　研究区概况

野外试验于青海省德令哈市怀头他拉试验基地开展,基地位于青海省德令哈市西北方向,地理位置为 96°44′E, 37°21′N,海拔为 2 869 m,属于干旱大陆性高原气候,多年平均气温为 4.1 ℃,日温差可达 25 ℃以上;多年平均降水量仅有 154.2 mm,且集中在 6、7 月份,多年平均蒸发量高达 2 301.5 mm。研究区位置见图 3。

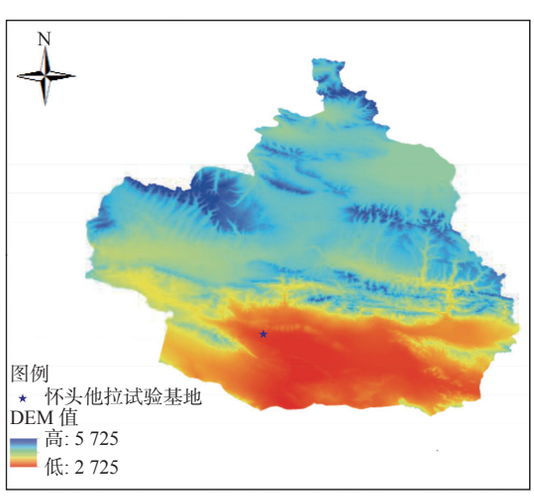

图 3　试验区位置

Fig. 3　Location map of the experimental area

2.2.2　试验方法

野外试验即开挖沙沟(20 cm),填沙,覆盖土石混合介质(10 cm),沙沟间种植植物。试验设置人工分层配土(ALS)处理组和野外实际原状土(Field Undisturbed Soil, FUS)对照组,见图 1,对于 ALS 处理组,在地表以下 5、20、40、60、85 cm 和沙土层 10 cm 处设置 TDR 水分温度自动观测系统,用以测定土壤 0~10 cm、31~50 cm、51~70 cm、71~100 cm 和

沙土层 11~30 cm 深度处的含水量，而 11~30 cm 处土壤含水量根据地表下 20 cm 和沙土层 10 cm 处的水分数据加权平均确定；对于 FUS 对照组，在地表下 10、30、50、70、90 cm 处安装 TDR 水分温度自动观测系统，测定 0~20 cm、21~40 cm、41~60 cm、61~80 cm、81~100 cm 的土壤含水量。

试验进行了原状土不同土层土壤基本物理性质的测定（表 2），该试验基地土壤中存在大量碎石，碎石比例呈现向下增大的趋势，地表 60 cm 以下为风化基岩层，难以保水。人工分层配土所需土壤、沙土和碎石就地取材获得，其中沙土为当地沙场粉碎沙，成本较低（为 6 元/m^3）。

表 2　不同土层土壤物理性质

Tab. 2　Soil physical properties of different soil layers

土层深度/cm	土壤干密度/(g·cm^{-3})	饱和含水率/%	土壤颗粒组成/%		
			黏粒（<0.002 mm）	粉粒（0.002~<0.05 mm）	砂粒（0.05~2.00 mm）
0~20	1.60	32	19.03	25.99	54.98
21~40	1.70	30	15.91	26.89	57.20
41~60	1.85	24	13.88	20.27	65.85
61~100	2.10	14	6.80	13.27	79.93

2.3　数据处理

土石混合介质中碎石的存在会改变土壤的水分特征，Peck 等[29] 引入碎石体积比例系数 R_v，提出碎石体积比例系数 R_v 与饱和导水系数间的关系，具体为

$$K_{st}=\frac{2(1-R_v)}{2+R_v}K_s \quad (1)$$

式中：K_s 为细土导水系数，cm/min；K_{st} 为土石混合介质饱和导水系数，cm/min；R_v 为碎石体积比例系数，取值为 0 ~ 1，当土壤无碎石时，R_v=0。

针对野外试验，计算土壤储水量为

$$W=\sum^{n}\theta_i H_i \quad (2)$$

式中：W 为土壤储水量，mm；i 为不同深度的土壤节点编号；n 为土层数；θ_i 为第 i 层土壤体积含水量，%；H_i 为每层土壤厚度，mm。本试验土壤深度为 0~100 cm，分为 5 层（n=5）。

利用水量平衡法计算该试验区的耗水量，方程为

$$\Delta W=W_i-W_j \quad (3)$$

$$ET=P+I+K-\Delta W-D-R \quad (4)$$

式中：ET 为试验区耗水量，mm；ΔW 为 0~100 cm 土壤储水变化量，mm；P 为降雨量；I 为灌溉水量，mm；K 为地下水补给量，mm；D 为深层渗漏水，mm；R 为地表径流量，mm；W_i、W_j 为某阶段土壤初始和结束时的储水量，mm。由于本试验无灌溉设计，故 I=0；试验区四周由隔离带隔开（高 20 cm），试验期间无地表径流产生，故 R=0；试验区降水少，土层较干，一次降水很难穿透土壤层，降水入渗主要储存在土壤层，故 D 忽略不计；由于试验区地下水埋藏较深，故可忽略地下水补给量（K）。因此在本试验中，研究区的水分注入项主要是降雨（P），输出项主要是耗水量 (ET)。

3　结果与讨论

3.1　室内试验

3.1.1　土壤水分入渗过程

不同处理组土壤水分入渗速率随时间的变化过程见图 4，在整个入渗过程中，不同处理组入渗速率变化趋势相同，均表现为随着时间的延长，入渗速率先迅速降低最后趋于稳定。对不同处理的入渗速率变化过程（表 3）分析可知，ALS 的初始入渗速率和平均入渗速率均显著高于 NLS。ALS 和 NLS 的初始入渗速率分别为 1.00 和 0.33 cm/min，提高了 3 倍以上。ALS 的平均入渗率较 NLS 提高了 67.57 %。这是由于 ALS 的土石混合介质在静止风干过程中产生了大量的大孔隙，促进了优先流的形成[30]，且这些大孔隙与沙沟中的沙土联通。在入渗过程中，尽管土石混合介质基质区导水性很小，可以忽略不计，但这些大孔隙可以将入渗水分快速渗入沙沟，沙土导水性很大，因此可以快速承接并储存上层土壤来水，同时将入渗水分快速补给下层土壤。另外，由于土壤具有膨胀性，在湿胀干缩过程中也将产生大量干缩裂隙，这些干缩裂隙也增大了土壤入渗能力[31]。在入渗后期，由于入渗水分可能已经将沙沟饱和，入渗能力由下层土壤控制，因此，

ALS 与 NLS 入渗能力相同,具有相近的稳定入渗速度。

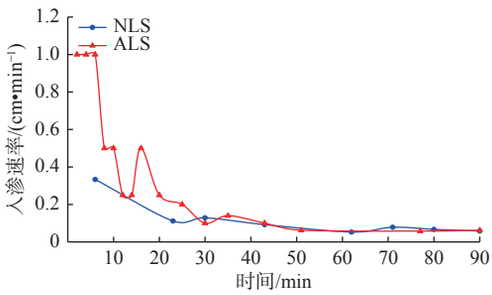

图 4　土壤水分入渗速率随时间的变化过程

Fig. 4　Relationship between soil infiltration rate and time

表 3　不同处理土壤水分入渗速率

Tab. 3　Soil infiltration rate of different treatments

处理组	初始入渗速率/(cm·min^{-1})	稳定入渗速率/(cm·min^{-1})	平均入渗速率/(cm·min^{-1})
NLS	0.33	0.058	0.12
ALS	1.00	0.062	0.37

结合土壤水分累计入渗量变化过程(图 5)来看,土壤水分累计入渗量都随时间的增大而单调增大。由于入渗前期人工分层配土(ALS)的入渗速率较快,因此入渗开始时累计入渗量涨幅较大,显著高于均质无分层土壤(NLS)的累计入渗量。但随着入渗时间的增加,累计入渗量斜率不再变化,累计入渗量增加的幅度较小。土壤水分入渗过程到达 90 min 时,试验处理 ALS、NLS 的累计入渗量分别为 16.8 和 8.88 cm,ALS 的累计入渗量较 NLS 增加 47.14 %。

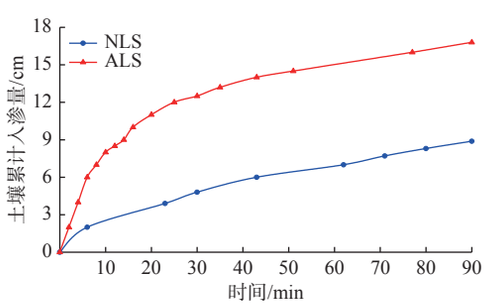

图 5　土壤水分累计入渗量变化过程

Fig. 5　Relationship between cumulative soil infiltration volume and time

碎石能够促进土壤水分的运动,同时碎石绕流作用明显,径流路径延长,从而阻碍水分运动,两者作用主要受碎石含量影响[32]。本试验碎石体积比例系数为 0.35,由公式(1)计算可得,试验中土石混合介质导水系数为细土导水系数的 0.55 倍。这说明土壤中含有碎石,会降低基质区入渗能力。相关研究与温明霞[33]、马翠丽等[34]研究结果相同。但实际入渗过程中,入渗初期 ALS 土壤入渗能力远大于 NLS,入渗后期两者基本相当。原因在于:入渗前期土石混合介质在静止风干过程中产生大量裂隙和大孔隙,形成优先流,增大了导水性;入渗后期,下层细土决定了入渗过程,因此两者基本相同。

3.1.2　土壤含水量变化过程

土壤剖面不同深度处含水量变化过程见图 6。可以看出,各土层土壤水分具有一致的动态变化规律,即所有深度土壤含水量均呈现因植被耗水和土壤蒸发而逐渐降低,灌水后急剧增加的变化过程。相同时间内,ALS 处理条件下,沙土层含水量最小,大部分时间位于沙土毛管断裂含水量以下(0.05 cm^3/cm^3),表层 0~10 cm 土壤含水量次之,31~40 cm 处含水量最大;而 NLS 处理的土壤条件下,各土层含水量相差较小。两者比较而言,ALS 的表层 0~10 cm 处土壤含水量远小于 NLS,这是由于 ALS 处理中,表层土壤由于碎石的存在,占据了大量土壤体积,降低了含水量。该结果与韩春苗等[35]研究结果一致,即细土中混有碎石会降低土壤含水量。结合灌水前后土壤剖面含水量情况(图 7)可以看出,灌水后,表层(0~10 cm)NLS 含水量增大至 0.272 cm^3/cm^3,ALS 含水量为 0.221 cm^3/cm^3,而深层(31~40 cm)NLS 含水量仅为 0.277 cm^3/cm^3,ALS 含水量高达 0.347 cm^3/cm^3,这表明 ALS 显著提高了土壤的下渗能力,快速补给了深层土壤含水量。另外,土石混合介质所形成的大孔隙和干缩裂隙促进了水分的快速下渗,也间接导致表层土壤获得较少下渗补给水量。沙土层中,除了灌水或灌水后一段时间内含水量较大外,大部分时间土壤含水量小于残余含水量(0.05 cm^3/cm^3),原因在于沙土持水能力较小,灌水后期沙土薄膜水可能以水汽扩散形式消耗于土壤蒸发。11~20 cm 土层中的平均含水量低于 21~30 cm 的,这是由于两层土壤含水量均采用面积加权平均法计算了土壤平均含水量,且在 11~20 cm 土层中沙土所占权重较大。同时,由图 6 可以看出,与 NLS 相比,ALS 含水量变化趋势较为缓慢,这可能是因为 ALS 中蒸散发耗水速度较慢,故水分运动较为缓慢。

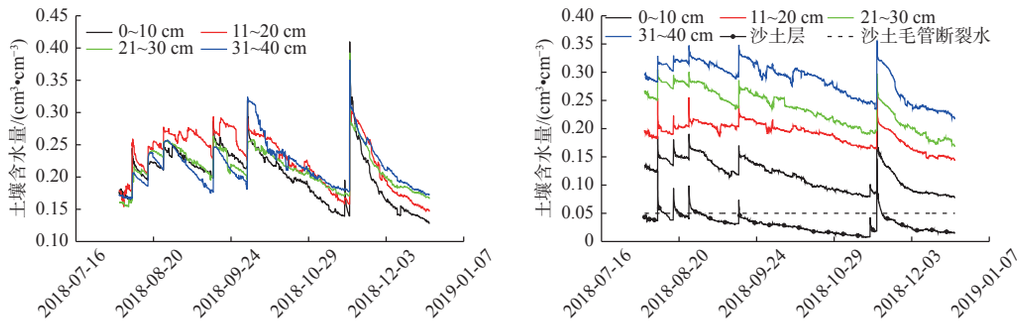

(a) 均质无分层土壤 (NLS)　(b) 人工分层配土 (ALS)

图 6　土壤含水量变化过程

Fig. 6　Variation of soil moisture content over time

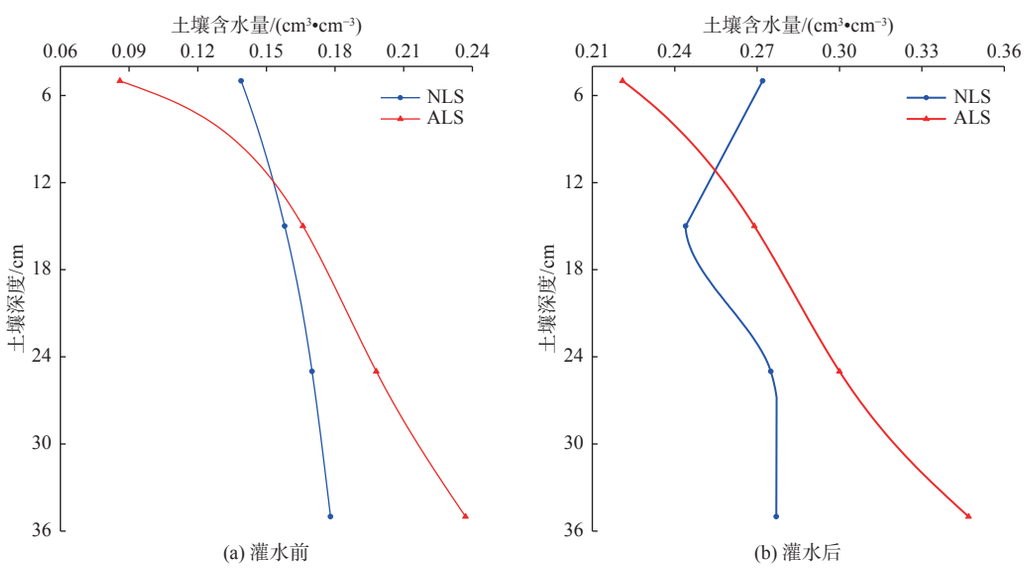

(a) 灌水前　(b) 灌水后

图 7　灌水前后土壤剖面含水量

Fig. 7　Soil profile moisture content before and after irrigation

3.1.3　土壤蒸散发量变化过程

土壤蒸散发包括植被蒸腾和土壤蒸发，本研究土柱中所种植吊兰同龄、同大小，因此在蒸散发计算过程中认为植被蒸腾相同，耗水差异主要来源于土壤蒸发。植被耗水试验土壤蒸散发动态过程见图 8，相同时间内，均质无分层土壤蒸散发量显著高于人工分层配土蒸散发量。在观测期内，NLS 日均蒸散发量为 4.35 mm，ALS 日均蒸散发量为 2.68 mm，故 ALS 降低了土壤的无效蒸发量，大约降低 38.39 %。原因在于：

土壤蒸散发过程中，一部分土壤水分通过植被根系吸水，最后通过叶面消耗于植物蒸腾；另一部分土壤水分，在毛细力作用下从湿润区向干燥区运移，并在土壤表面消耗于土壤蒸发。大量研究表明，当土壤毛管连通性破损后，液态形式的水分运移基本停止[36]。土壤中液态水可以分为毛管水和薄膜水，通常薄膜水被认为不影响水分的运移过程，用剩余(残余)含水率代替[37]。结合图 6(b)，可以看出大部分时间内，沙土层的水分低于剩余含水量，这说明大部分时间沙土层毛管水处于断裂状态，深层土壤水分无法通过毛管水上升补给表层土壤。

人工分层配土处理中表层土壤中混有大量碎石，降低了表层土壤持水能力和基质区土壤导水能力，从而有利于降低土壤蒸发。同时因为沙土层阻断了毛管上升通道，表层土壤难以得到深层土壤水分补给，造成表层土壤长期处于干燥状态，因而在蒸散发过程中进一步降低了土壤无效蒸发，这与董荣泽等[38]研究结论一致。

均质无分层土壤由于表层不存在碎石和沙土隔水层，则在非灌水期，一部分水分消耗于植被蒸腾，另一部分水分在毛管力作用下不断将深层土壤水分运移到土壤表面并消耗于土壤无效蒸发，从而增大了土壤的无效蒸发，加大了土壤总蒸发量。

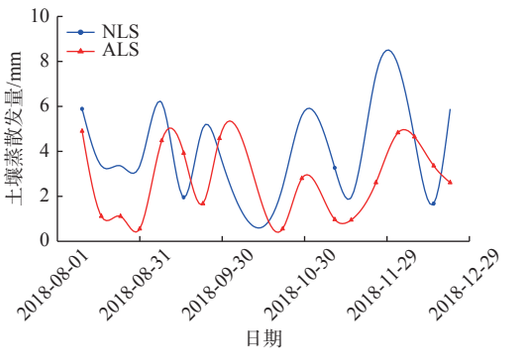

图 8　土壤蒸散发量变化过程

Fig. 8　The process of soil evapotranspiration over time

3.2　野外试验

3.2.1　土壤含水量时间动态过程

不同深度土壤含水量随时间变化过程见图 9。可以看出：相同时间内，野外原状土(FUS)对照组表层 0~20 cm 土壤含水量最高，并且随着土层深度增加含水量逐渐降低；相较于对照组，ALS 处理组，31~50 cm 土层含水量最高，0~10 cm 表层土壤含水量显著小于 FUS。这可能是由于 ALS 表层土壤中的大量碎石占据了土壤体积，大幅降低了土壤持水能力[39]，且沙土对地下水的补给有一定的延缓、抑制作用，从而降低沙土上层土壤的含水量[40-41]。由于沙土导水能力较强，ALS 中 31~50 cm 土壤含水量明显提升，这与宋日权等[42]的土壤掺砂可显著提高掺砂层以下土壤的含水率结论相同。

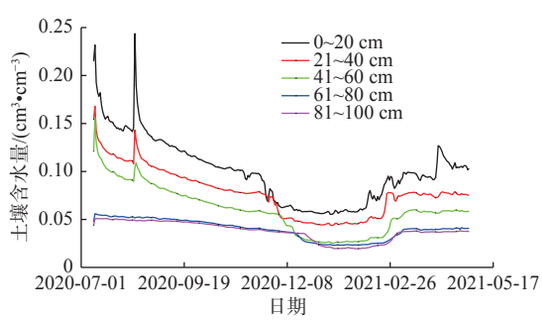

(a) 野外原状土壤 (FUS 对照组)

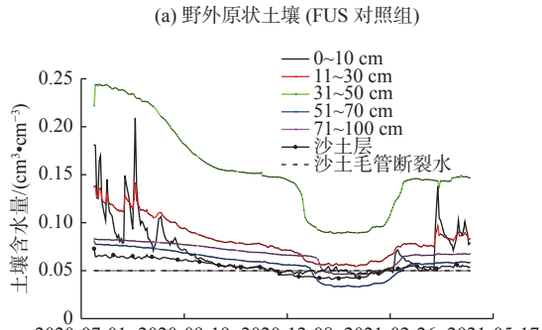

(b) 人工分层配土 (ALS 处理组)

图 9　土壤含水量随时间变化过程

Fig. 9　Schematic diagram of the dynamic change of soil water content with time

3.2.2　土壤含水量垂直变化过程

不同处理措施土壤含水量(平均值)垂直变化过程见图 10。FUS 对照组土壤含水量随深度的增加，呈现先减少后稳定的趋势，而 ALS 处理组土壤含水量随土层深度增加，呈现减少—增加—减少，最后趋向稳定的趋势。结合图 9，0~30 cm 土壤含水量为 FUS 高于 ALS，30 cm 以下 ALS 土壤含水量高于 FUS，且 FUS 表层土壤含水量最高而 ALS 在 31~50 cm 土层处含水量最高。这是由于土石混合介质形成大量干缩裂隙和沙土促进水分快速下渗，提高了土壤的入渗能力，且沙土可以有效阻断毛孔吸力，维持表层土壤干燥状态，使水分储存在下层土壤中供植物生长利用，进而减少土壤的无效蒸发。

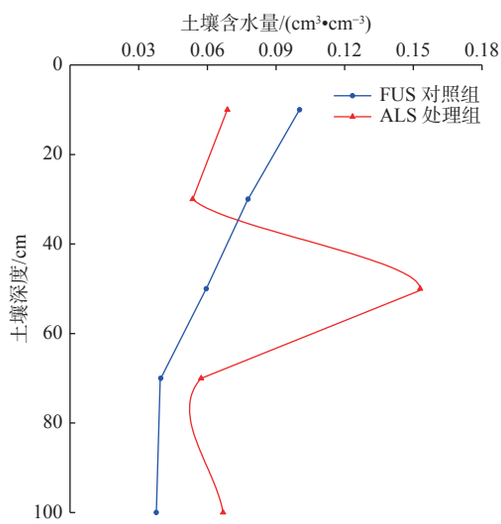

图 10　不同处理措施土壤含水量垂直变化过程

Fig. 10　Vertical changes of soil moisture under different treatments

3.2.3　水量平衡分析

根据公式(2)计算土壤储水量，见图 11。可以看出，不同处理方式土壤储水量均随着时间波动。FUS 对照组土壤储水量随着深度的增加逐渐减小，水分主要储存在土壤表层，而 ALS 处理组土壤储水量主要储存于地表以下 31~50 cm。

根据公式(3)、(4)，可计算出该试验区耗水量，计算时间为 2020 年 7 月—2020 年 10 月，结果见表 4。ALS 土壤总储水变化量为−38.78 mm，而 FUS 为−51.70 mm，大约增加 24.99 %。同时 ALS 耗水量为 84.08 mm，较 FUS 大约降低 13.32 %。7 月和 8 月，FUS 的耗水速率显著高于 ALS，这是因为 7、8 月降雨量较多，FUS 水分主要储存于表层土壤，蒸发较大，而 ALS 由于沙土促进水分快速下渗及其毛管阻断作用，表层土壤含水量较低，减小了土壤的

无效蒸发；9 月和 10 月，由于气候变化，降雨量骤减，而 ALS 由于水分主要储存在较深层土壤，无效蒸发较小，土壤中水分含量较高，故耗水速率偏高。计算期内，FUS 总耗水速率为 0.93 mm/d，ALS 为 0.81 mm/d。

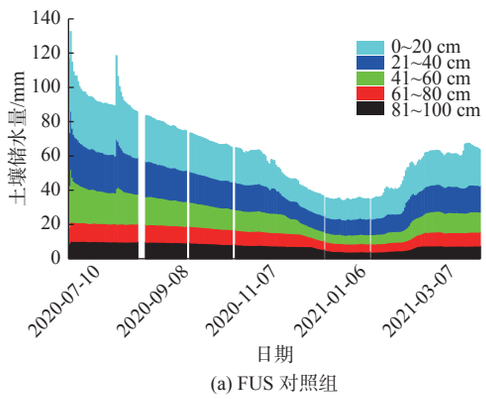

(a) FUS 对照组

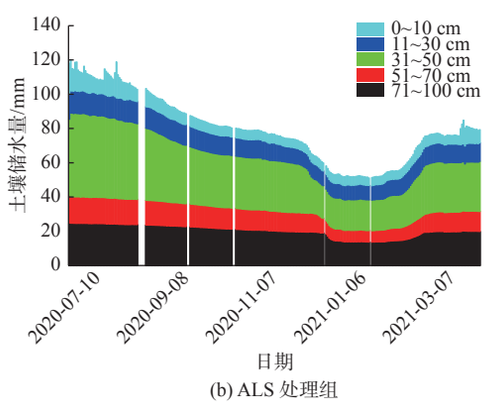

(b) ALS 处理组

图 11　不同处理方式的土壤储水量

Fig. 11　Soil water storage capacity of different treatment methods

表 4　不同处理方式土壤水量平衡分析

Tab. 4　Soil water balance with different treatment methods

时间	降雨量/mm	FUS对照组			ALS处理组		
		储水量变化/mm	耗水量/mm	耗水速率/(mm·d^{-1})	储水量变化/mm	耗水量/mm	耗水速率/(mm·d^{-1})
2020-07	21.40	−25.41	46.81	2.23	−9.80	31.20	1.49
2020-08	20.90	−9.45	30.35	1.17	−5.88	26.78	1.03
2020-09	2.10	−8.53	10.63	0.38	−14.67	16.77	0.60
2020-10	0.90	−8.31	9.21	0.31	−8.43	9.33	0.32
合计	45.30	−51.70	97.00	0.93	−38.78	84.08	0.81

4　结 论

人工分层配土本质为改变土壤原有组合方式，提高土壤的入渗能力，通过影响水分运移来影响土壤含水量，从而改变土壤水分分布特征。本研究运用人工分层配土措施开展室内及野外试验，得出如下结论：

在积水入渗试验中，与均质无分层处理相比，人工分层配土初期入渗速率提高 3 倍以上，显著加快水分初始下渗速度。在入渗后期，由于沙土层达到饱和状态，人工分层与均质无分层的土壤入渗能力基本稳定且相近。人工分层配土平均入渗率较无分层提高 67.57 %，累计入渗量增加 47.14 %。在人工分层配土中，沙土含水量最低，而 30~40 cm 土层含水量最高，而均质无分层处理的土壤条件下，各土层含水量相近。

在植被耗水试验中，人工分层配土处理后，由于表层土壤持水能力下降且沙土层阻断了毛管上升通道，降低 38.39 % 的土壤无效蒸发量。

在野外观测试验中，原状土在 0~20 cm 土层含水量最高，而人工分层配土土壤含水量主要储存于地表以下 31~50 cm 处，表层土壤含水量显著低于原状土。人工分层配土土壤储水变化量较原状土提高 24.99 %，耗水量减少 13.32 %，总耗水速率明显降低。

人工分层配土措施主要用于极端干旱区绿化，工程施工简单，所需细土、碎石和沙土均是自然界土石材料，取材方便，且人工分层处理后，只要不对土层结构进行破坏，处理一次便可长久使用，因此具有大规模推广应用价值。

参考文献：

[1] ZHAO J L, YANG Z Q, GOVERS G. Soil and water conservation measures reduce soil and water losses in China but not down to background levels: Evidence from erosion plot data[J]. Geoderma, 2019, 337: 729-741. DOI: 10.1016/j.geoderma.2018.10.023.

[2] 刘燕青, 王计磊, 李子忠. 秸秆覆盖对土壤水分和侵蚀的影响研究进展[J]. 水土保持研究, 2021, 28(6): 429-436. DOI: 10.13869/j.cnki.rswc.2021.06.036.

[3] 刘粲. 黄土高原植被恢复对土壤水分的影响研究[D]. 石家庄: 河北地质大学, 2022. DOI: 10.27752/d.cnki.gsjzj.2022.000534

[4] 赵瑞. 沙漠修复植物生态适应性评价及系统研发[D]. 泰安: 山东农业大学, 2018.

[5] ZOU H, GAO G Y, YUAN C A. Interactions between soil water and plant community during vegetation succession in the restored grasslands on the Loess Plateau of China[J]. Land Degradation & Develop-

ment, 2022, 34(5): 1582-1592. DOI: 10.1002/LDR.4555.

[6] 杨凯悦. 高寒沙区柠条人工林光合耗水特性及影响因素研究[D]. 北京: 中国林业科学研究院, 2019. DOI: 10.27625/d.cnki.gzlky.2019.000023

[7] 杜康, 张北赢. 黄土丘陵区不同土地利用方式土壤水分变化特征[J]. 水土保持研究, 2020, 27(6): 72-76. DOI: 10.13869/j.cnki.rswc.2020.06.010.

[8] 李高亮, 王科, 段翠花, 等. 黄土丘陵区降雨后鱼鳞坑土壤水分动态模拟研究[J]. 水土保持研究, 2022, 29(2): 76-84+91. DOI: 10.13869/j.cnki.rswc.20210630.002.

[9] 谢成俊, 王平, 陈娟. 不同覆盖方式对农田土壤水热状况及马铃薯产量的影响[J]. 土壤通报, 2019, 50(5): 1151-1158. DOI: 10.19336/j.cnki.trtb.2019.05.20.

[10] 刘宇奇, 朱雪峰, 鲍雪莲, 等. 玉米秸秆覆盖还田量对黑土微生物碳代谢活性与多样性的影响[J]. 土壤通报, 2023, 54(2): 407-415. DOI: 10.19336/j.cnki.trtb.2022101902.

[11] CHE Z, WANG J, LI J S. Effects of water quality, irrigation amount and nitrogen applied on soil salinity and cotton production under mulched drip irrigation in arid northwest China[J]. Agricultural Water Management, 2021, 247: 106738. DOI: 10.1016/j.agwat.2021.106738.

[12] 甘永德, 贾仰文, 仇亚琴, 等. 降雨条件下分层土壤入渗特性[J]. 水土保持学报, 2012, 26(5): 217-219,223. DOI: 10.13870/j.cnki.stbcxb.2012.05.027.

[13] GAN Y D, LI H, JIA Y W, et al. Infiltration-runoff model for layered soils considering air resistance and unsteady rainfall[J]. Hydrology Research, 2018, 50(2): 431-458. DOI: 10.2166/nh.2018.007.

[14] 邓超, 苏南, 曹子聪, 等. 不同类型土壤裂隙特征研究[J]. 农业与技术, 2022, 42(19): 90-93. DOI: 10.19754/j.nyyjs.20221015022.

[15] 司曼菲, 甘永德, 刘欢, 等. 土石混合介质碎石性质对土壤入渗和产流过程影响[J]. 南水北调与水利科技, 2018, 16(2): 59-63. DOI: 10.13476/j.cnki.nsbdqk.2018.0039.

[16] 李建明, 孙蓓, 王一峰, 等. 矿区3种弃土弃渣体侵蚀及水动力学差异研究[J]. 长江科学院院报, 2017, 34(10): 24-30. DOI: 10.11988/ckyyb.20160667.

[17] 赵满, 王文龙, 郭明明, 等. 不同砾石含量墁土堆积体坡面侵蚀特征研究[J]. 土壤学报, 2020, 57(5): 1166-1176. DOI: 10.11766/trxb201905220129.

[18] 甘凤玲, 何丙辉, 王涛. 汶川震区滑坡堆积体降雨入渗产流特征人工模拟实验研究[J]. 水利学报, 2016, 47(6): 780-788. DOI: 10.13243/j.cnki.slxb.20150927.

[19] 尤今, 王树谦. 土壤裂隙对农田土壤优先流的影响及其控制因子[J]. 节水灌溉, 2022(9): 71-75,80.

[20] 吕文聪, 邱阳, 谢忠奎, 等. 砾石覆盖粒径对土壤入渗过程的影响[J]. 水土保持研究, 2021, 28(6): 46-51. DOI: 10.13869/j.cnki.rswc.2021.06.004.

[21] 周蓓蓓, 邵明安. 不同碎石含量及直径对土壤水分入渗过程的影响[J]. 土壤学报, 2007(5): 801-807. DOI: 10.3321/j.issn:0564-3929.2007.05.005.

[22] 邵丽媛, 甘永德, 苏辉东, 等. 土壤膨胀性对降雨入渗产流影响试验[J]. 中国农村水利水电, 2018, 11: 42-54. DOI: 10.3969/j.issn.1007-2284.2018.11.009.

[23] COPPOLA A, COMEGNA A, DRAGONETTI G, et al. Simulated preferential water flow and solute transport in shrinking soils[J]. Vadose Zone Journal, 2015, 14(9): 1-22. DOI: 10.2136/vzj2015.02.0021.

[24] COPPOLA A, GERKE H H, COMEGNA A, et al. Dual-permeability model for flow in shrinking soil with dominant horizontal deformation[J]. Water Resources Research, 2012, 48(8): W08527. DOI: 10.1029/2011WR011376.

[25] 甘永德, 刘欢, 贾仰文, 等. 膨胀性土壤饱和水分运动参数计算模型[J]. 工程科学与技术, 2018, 50(2): 77-83. DOI: 10.15961/j.jsuese.201700680.

[26] 汪顺生, 翟士旭, 傅渝亮, 等. 含砂层层位及厚度变化条件下层状土上升毛管水运动特性研究[J]. 灌溉排水学报, 2019, 38(11): 49-57. DOI: 10.13522/j.cnki.ggps.20190048.

[27] 贾振江, 刘学智, 徐天渊, 等. 砂土混合覆盖下的土壤水分蒸发特性及其因子分析[J]. 水土保持学报, 2023, 37(2): 227-236. DOI: 10.13870/j.cnki.stbcxb.2023.02.026.

[28] 王全九, 汪志荣, 张建丰, 等. 层状土入渗机制与数学模型[J]. 水利学报, 1998(S1): 77-80. DOI: 10.13243/j.cnki.slxb.1998.s1.017.

[29] PECK A J, WATSON J D. Hydraulic conductivity and flow in non-uniform soil[C]. Workshop on Soil Physics and Field Heterogeneity, CSIRO Div. of Environmental Mechanics, Canberra, Australia, 1979: 31-39.

[30] 苏辉东, 赵思远, 贾仰文, 等. 崇陵流域土石山区坡面优先流发育路径研究[J]. 水文, 2019, 39(6): 1-6.

DOI: 10.19797/j.cnki.1000-0852.20180304.

[31] 王策, 张展羽, 陈晓安, 等. 基于水量平衡原理的裂隙优先流双域渗透模型及其应用[J]. 农业机械学报, 2021, 52(10): 314-326, 348. DOI: 10.6041/j.issn.1000-1298.2021.10.033.

[32] 房凯, 郑加兴, 张俐, 等. 砾石覆盖对土壤入渗特性影响的试验研究[J]. 中国农村水利水电, 2020(2): 100-104. DOI: 10.3969/j.issn.1007-2284.2020.02.020.

[33] 温明霞. 不同土石混合介质水分运动的试验研究[D]. 杨凌: 西北农林科技大学, 2011.

[34] 马翠丽, 吕世华, 潘永洁, 等. 砾石参数化对青藏高原陆面过程模拟的影响及敏感性分析[J]. 高原气象, 2020, 39(6): 1219-1231. DOI: 10.7522/j.issn.1000-0534.2020.00005.

[35] 韩春苗, 甘永德, 贾仰文, 等. 土石混合介质中碎石性质对土壤水分特征曲线的影响分析[J]. 中国农村水利水电, 2018(8): 86-90. DOI: 10.3969/j.issn.1007-2284.2018.08.018.

[36] 邵明安, 王全九, 黄明斌. 土壤物理学[M]. 北京: 高等教育出版社, 2006.

[37] VAN GENUCHTEN M T, LEIJ F J, WU L. Characterization and measurement of the hydraulic properties of unsaturated porous media (parts 1 and 2) [C] // Proceedings of the International Workshop, Riverside, Calif. , 1997, 22–24.

[38] 董荣泽, 于明英, 邱照宁, 等. 沙土上升毛管水运动特性研究[J]. 节水灌溉, 2018(4): 19-25. DOI: 10.3969/j.issn.1007-4929.2018.04.005.

[39] BOUWER H, RICE R C. Hydraulic properties of stony vadose zone[J]. Ground Water, 1984, 22(6): 696-705. DOI: 10.1111/j.1745-6584.1984.tb01438.x.

[40] 贾俊超, 张兴昌. 层状土持水性室内模拟初步研究[J]. 水土保持研究, 2020, 27(6): 90-93,99. DOI: 10.13869/j.cnki.rswc.2020.06.013.

[41] CHEN S, MAO X M, BARRY D A, et al. Model of crop growth, water flow, and solute transport in layered soil[J]. Agricultural Water Management, 2019, 221: 160-174. DOI: 10.1016/j.agwat.2019.04.031.

[42] 宋日权, 褚贵新, 冶军, 等. 掺砂对土壤水分入渗和蒸发影响的室内试验[J]. 农业工程学报, 2010, 26(S1): 109-114.

• 译文 •

Experiment on water and soil regulation method based on layered soil

ZHENG Liping[1]，GAN Yongde[1]，JIA Yangwen[2]，WU Yushuai[1]，LIU Huan[2]，YUAN Riping[1]

（1. *School of Water Conservancy and Electric Power, Qinghai University/Laboratory of Ecological Protection and High Quality Development of the Upper Yellow River, Xining* 810016, *China*；2. *State Key Laboratory of Simulation and Regulation of Water Cycles in River Basin, China Institute of Water Resources and Hydropower Research, Beijing* 100038, *China*）

Abstract: With the guidance of soil physics principles and the utilization of fundamental physical properties of soil, a technology called artificially layered soil (ALS) engineering was proposed to achieve water and soil regulation by adjusting the soil profile. Experiments of laboratory infiltration ponding, vegetation evapotranspiration, and field soil moisture observation in arid areas were conducted to verify the effectiveness of ALS in water and soil regulation. The results show that in these experiments, by adjusting the soil profile structure, ALS can significantly improve the infiltration capacity of the soil, with the initial infiltration rate increasing by more than three times and the average infiltration rate increasing by 67.57%. Additionally, the cumulative soil infiltration volume increases by 47.14%. Meanwhile, the surface soil water content is decreased to reduce the invalid soil evaporation by 38.39%. In the field experiments, the soil water content in the layered soil is mainly stored at a depth of 31–50 cm below the surface, while that of the undisturbed field soil is mainly located in the surface soil. Compared with the undisturbed soil, ALS reduces water consumption by 13.32% and decreases the water consumption rate by 12.90%. Therefore, ALS engineering can realize water and soil regulation, making it significant for water and soil resource management and desertification prevention in arid regions.

Key words: soil physical property; layered soil; soil water content; soil evaporation; soil infiltration

Chinese Library Classification No. : TV213; S152 **Document Code:** A

In arid areas, in addition to rainfall scarcity, soil evaporation, and soil erosion also result in ineffective moisture loss, water shortage, and soil degradation [1-2]. Vegetation construction is a crucial component of ecological environment building, and vital in intercepting and retaining rainfall, reducing runoff, stabilizing soil, preventing erosion, and improving the ecological environment, vegetation serves as the hub of material circulation and energy exchanges in ecosystems, and the material basis for preventing ecological degradation [3]. Consequently, it plays a significant role in improving the ecological environment [4]. Soil moisture is an essential source for plant utilization and a necessary nutrient for survival and growth. It plays an irreplaceable part in physiological processes such as photosynthesis, respiration, and nutrient transport in plants, and is also a critical ecological limiting factor in vegetation construction [5-6]. In arid areas, natural rainfall is a primary source of soil moisture. Therefore, exploring effective soil and water regulation measures and utilizing existing rainwater to address afforestation challenges are of scientific significance for these areas.

The technology of drought-resistant afforestation and land preparation is a crucial foundation for afforestation in arid and semi-arid regions, significantly influencing the growth and development of tree species, with the main purpose of water storage and moisture conservation. The current land preparation specifically includes reverse slope horizontal ditches, reverse slope horizontal steps, horizontal steps, fish scale pits, and

Received: 2023-03-08 **Revised:** 2023-06-29

Online publishing address: http//:

Fund: National Natural Science Foundation of China (51909129); Major Science and Technology Projects in Qinghai Province (2021-SF-134)

Author's brief: ZHENG Liping (1997–), female, from Nanbu, Sichuan Province, is mainly engaged in the research on soil and water regulation in arid areas. E-mail: zlp113@qhu.edu.cn

Corresponding author: GAN Yongde (1985–), male from Minhe, Qinghai Province, is an associate professor and Ph.D., mainly engaged in research on watershed water cycle simulation, water and soil regulation in arid areas, and water resources planning and management. E-mail: bjganyd@163.com

plastic mulch [7-11], which are typically carried out manually or mechanically. In arid areas, in addition to the inherent low rainfall, the current land preparation techniques can not significantly address the low soil infiltration capacity and substantial ineffective soil evaporation. Therefore, efficient rainwater utilization remains challenging. Studies have shown that soil infiltration and evapotranspiration characteristics can be realized by improving soil physical properties and layering combinations [12-13]. Meanwhile, in natural conditions, due to the effects of soil expansibility, root systems, and insect burrows, numerous shrinkage cracks and large pores are developed in the soil, significantly influencing soil infiltration [14]. On one hand, gravel in the soil increases the proportion of pores in the soil [15-17], which leads to more pathways for water flow, the formation of preferential flow in large pores, an increase in the proportion of subsurface flow, and infiltration flow brought by rainfall, and a reduction in surface runoff [18-20]. On the other hand, gravel also increases the curvature of water flow and reduces the water passage area to hinder infiltration. Zhou et al. [21] found that the content and size of gravel determine the dominant proportion of these two effects. Shrinkage cracks and large pores serve as the preferential flow pathways for rainwater to enter the soil during rainfall periods [22-25], facilitating rapid rainwater infiltration. Sandy soil features strong hydraulic conductivity and weak water retention capacity, thus enabling rapid moisture infiltration and storage during rainfall events. At the same time, Shi et al. [26] found that sandy soil layer can suppress the speed and height of capillary water rise. Therefore, compared with homogeneous soil, sandy layers retain moisture in the lower soil layers, which significantly prolongs the time needed for the upper soil layers to reach a certain water content and affects the surface soil water content. Therefore, sandy soil can restrain soil evaporation capacity [27], thereby reducing ineffective soil evaporation.

Previous studies focused on the individual effects of soil-rock mixed media and interbedded sand layers on moisture movement. In this study, soil-rock mixed media and sandy soil were combined, and soil layering [28], soil expansibility, and other basic physical properties were utilized to adjust the soil structure. A quantitative analysis of the impact of ALS on soil hydrological processes such as infiltration, soil moisture redistribution, and evapotranspiration was conducted. The aim is to enhance the soil infiltration capacity and reduce ineffective soil evaporation based on economic and environmental protection, which helps store soil moisture in deeper layers for plant utilization and maintaining surface soil at a lower water content. Finally, soil and water regulation is realized to provide technical and theoretical support for the ecological environment restoration and management in arid areas.

1 ALS design

Based on reference research and preliminary studies, relevant research on soil layering combinations and the impact of soil-rock mixed media on infiltration has been conducted. These influencing factors were also fully considered in ALS design. Therefore, by utilizing the physical properties of soil layering and soil-rock mixed media, the existing natural soil layering combinations can be modified to alter soil infiltration capacity and evapotranspiration, thus achieving soil and water regulation. The specific improvement measures are as follows:

For areas with a certain slope (5° –25°), the specific engineering involves digging sand ditches on the original soil surface, filling them with sand, and then covering the filled ditches with a layer of expansive soil-rock mixed media, as illustrated in Fig. 1. The newly modified soil consists of two new layers artificially configured on top of the original soil layers, altering the original layered combination of the soil. Therefore, it is called ALS engineering.

The soil-rock mixed media layer consists of soil and gravel, with the mass of gravel accounting for 40% of the total and the gravel particle size of 1–3 cm. The sand ditches are composed of sandy soil, and their cross-sections are elliptical in shape, with a long diameter of 1.5–2.0 m and a short diameter of 0.2–0.4 m. The adjacent sand ditches form a wavy line pattern, and vegetation is planted between the sand ditches.

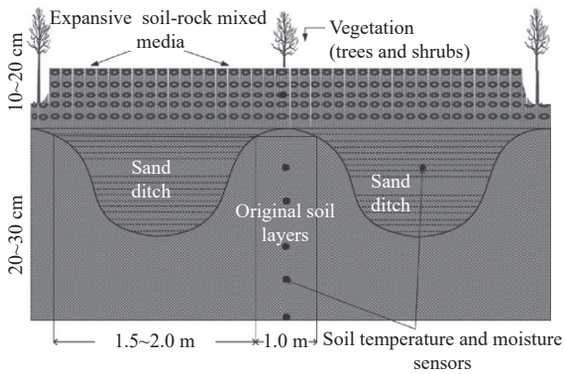

Fig. 1 Cross-section of ALS engineering

2 Materials and methods

2.1 Laboratory experiment

2.1.1 Experimental materials

The soil samples adopted in the experiment consisted of sandy soil, gravel (particle size of 1–3 cm), and loam. All the soil samples were air-dried and sieved for later utilization (loam sieved to 2 mm and sandy soil to 2 mm). The initial soil water content, dry bulk density, and saturated water content were determined by the oven-drying method. The soil particle composition was measured by the straw method, and the saturated hydraulic conductivity was by the constant head method. The results were presented in Tab. 1. The gravel in the experiment had a particle size ranging from 1 to 3 cm and was sourced from construction materials. The soil-rock mixed media was obtained by mixing loam and gravel, with the gravel accounting for 40% of the total mass. The water samples in the experiment were taken from indoor tap water.

Tab. 1 Basic physical properties of soil

soil type	density/ ($g \cdot cm^{-3}$)	saturated hydraulic conductivity/ ($cm \cdot min^{-1}$)	saturated water content/($cm^3 \cdot cm^{-3}$)	residual water content/($cm^3 \cdot cm^{-3}$)	distribution of soil diameter/%		
					>50 μm	2–50 μm	<2 μm
sandy soil	1.60	0.960	0.38	0.05	96.34	3.66	0
loam	1.36	0.064	0.42	0.06	38.06	40.01	21.93

2.1.2 Experimental method

The experiments were conducted in the Water Conservancy Hall Laboratory of Qinghai University through the vertical soil column method (with a column height of 60 cm and an inner diameter of 40 cm). The experiments included vertical one-dimensional infiltration ponding experiment and vegetation water consumption experiment. Each experiment had two treatments of ALS and homogeneous no-artificially layered soil (NLS), where NLS is homogeneous loam. The experimental setup consisted of soil columns, Mariotte bottles, weighing equipment, and data collector.

In the ALS treatment group, during soil filling, first, a layer of sand with an approximate thickness of 10 cm was laid at the bottom of the soil trough to serve as the anti-filtration layer. Then, a layer of gauze was placed on top of the sand. Loam, sandy soil, and soil-rock mixed media were filled in the soil trough following the soil layering sequence of ALS. The densities were 1.36 g/cm^3 for loam, 1.60 g/cm^3 for sandy soil, and 1.56 g/cm^3 for the soil-rock mixed media respectively. Due to the small diameter of the soil column, the sand ditches were narrowed (a parabolic shape) during soil filling, as shown in Fig. 2. To determine the soil water profiles, we installed EM50 soil temperature and moisture sensors at the center of the soil column at depths of 5 cm, 15 cm, 25 cm, 35 cm, and 7.5 cm of the sand layer corresponding to the 17.5 cm of the soil column. These sensors were employed to measure the soil water content at depths of 0–10 cm, 31–40 cm, and in the sandy soil layer at a depth of 0–15 cm. The soil water content at depths of 11–20 cm and 21–30 cm was determined by taking the weighted average of the soil water data at the center of the soil column at 15 cm and 25 cm respectively, along with the water data at the sandy soil layer at 7.5 cm.

In the homogeneous NLS treatment group, during soil filling, first, a layer of sand with an approximate thickness of 10 cm was laid at the bottom of the soil

trough to serve as the anti-filtration layer. Then, a layer of gauze was placed on top of the sand. Loam with a density of 1.36 g/cm^3 was filled in the soil trough following the natural soil composition. EM50 soil temperature and moisture sensors were installed at the center of the soil column at depths of 5 cm, 15 cm, 25 cm, and 35 cm to measure the soil water content profiles. These sensors were adopted to measure the soil water content at depths of 0–10 cm, 11–20 cm, 21–30 cm, and 31–40 cm respectively.

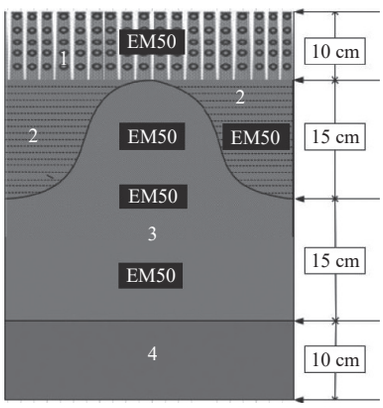

Note: 1.Soil-rock mixed media layer; 2.Sandy soil layer; 3.Loam layer; 4.Gravel layer.

Fig. 2 Soil profile for ALS experiment

A Mariotte bottle with constant pressure was leveraged for water supply during the experiment. The readings of the bottle and the depth of the infiltration pond in the soil column were measured during the experiment to calculate the cumulative soil infiltration volume over the period. Throughout the experimental period, the EM50 moisture sensor recorded the soil water content every 20 minutes.

Infiltration ponding experiment. Before experimenting, the soil trough was filled with enough water (the soil reaching above the field water holding capacity and generating significant subsurface flow). After air drying, the infiltration experiment was carried out. Water was supplied by a Mariotte bottle, and the infiltration duration was controlled to be approximately 90 minutes. The indoor temperature during this period was around 25 ℃. The main observed data included the readings of the Mariotte bottle and the infiltration duration.

Vegetation water consumption experiment. The employed soil filling method and instruments were the same as those in the infiltration experiment. As shown in Fig. 1, after the soil filling, a plant (one spider plant) was planted on the convex surface of the original soil layer (in the middle of the sand ditch). Subsequently, a significant amount of water was injected into the soil column (the soil reaching above the field water holding capacity and generating significant subsurface flow) to conduct the experiment. The experiment commenced on August 5, 2018, and concluded on December 22, 2018, with an indoor temperature of around 25 ℃ and indoor humidity at 15%. Watering was conducted every10-20days,andthesoilevapotranspirationwasmeasured by the weighing method (with a precision of 0.1 g). Measurements were taken once a week, and additional measurements were taken before and after each watering.

2.2 Field experiment

2.2.1 Overview of the study area

The field experiment was conducted at the Huaitoutala Experimental Base in Delingha City, Qinghai Province. The base is located in the northwest of Delingha City, Qinghai, with a geological location of 96°44′E and 37°21′N, and an elevation of 2 869 meters above sea level. The area is characterized by a dry continental plateau climate, with an average annual temperature of 4.1℃ and a diurnal temperature difference exceeding 25℃. The annual average precipitation is only 154.2 mm which is concentrated mainly in June and July, while the average annual evaporation is as high as 2 301.5 mm. The location of this area is shown in Fig. 3.

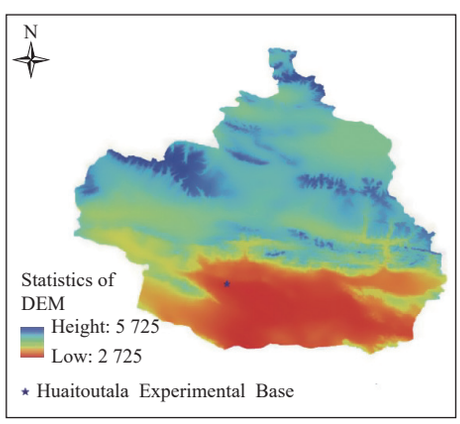

Fig. 3 Location of the experimental area

2.2.2 Experimental method

The field experiment involved excavating sand ditches (20 cm), filling them with sand, and covering

them with soil-rock mixed media (10 cm). Vegetation was planted between the sand ditches. The experiment consisted of two groups including the ALS treatment group and the field undisturbed soil (FUS) control group (Fig. 1). For the ALS treatment group, TDR (time domain reflectometry) soil moisture and temperature automatic observation systems were installed at depths of 5 cm, 20 cm, 40 cm, 60 cm, and 85 cm below the surface, and 10 cm in the sandy soil layer. These systems were utilized to measure the soil water content at depths of 0–10 cm, 31–50 cm, 51–70 cm, 71–100 cm, and 11–30 cm in the sandy soil layer. The soil water content at the depth of 11–30 cm was determined by taking the weighted average of the moisture data at 20 cm below the surface and 10 cm of the sandy soil layer. For the FUS control group, TDR soil moisture and temperature automatic observation systems were installed at depths of 10 cm, 30 cm, 50 cm, 70 cm, and 90 cm below the surface to measure the soil water content at depths of 0–20 cm, 21–40 cm, 41–60 cm, 61–80 cm, and 81–100 cm.

The experiment involved measuring the basic physical properties of various soil layers in undisturbed soil (Tab. 2). A large quantity of gravel existed in the soil of the experimental base, and its proportion increases with depth. There was a wind-weathered bedrock layer below 60 cm from the surface, which posed challenges to water retention. The soil, sandy soil, and gravel required for ALS treatment were obtained locally, with the low-cost sandy soil sourced from a local sand quarry (price of 6 yuan/m^3).

Tab. 2 Soil physical properties of different soil layers

soil depth/cm	dry density of soil/ ($g \cdot cm^{-3}$)	saturated water rate/%	soil particle composition/%		
			size of loam (<0.002 mm)	size of silt (0.002–<0.05 mm)	size of sand (0.05–2.00 mm)
0–20	1.60	32	19.03	25.99	13.27
21–40	1.70	30	15.91	25.99	57.20
41–60	1.85	24	13.88	25.99	65.85
61–100	2.10	14	6.80	13.27	79.93

2.3 Data processing

Gravel in the soil-rock mixed media can alter the soil moisture characteristics. Peck et al. [29] introduced the gravel volume ratio coefficient R_v and proposed the relationship between R_v and saturated hydraulic conductivity. Specifically, it is expressed as follows:

$$K_{st} = \frac{2(1-R_v)}{2+R_v} K_s \quad (1)$$

where K_s is the hydraulic conductivity of fine soil (unit: cm/min); K_{st} is the saturated hydraulic conductivity of the soil-rock mixed media (unit: cm/min); R_v is the gravel volume ratio coefficient ranging from 0 to 1. When the soil contains no gravel, R_v=0.

For the field experiment, the calculated soil water storage capacity is as follows:

$$W = \sum_{i}^{n} \theta_i H_i \quad (2)$$

where W is the soil water storage capacity (unit: mm); i is the soil node number at different depths; n is the number of soil layers; θ_i is the volumetric water content of the ith layer of soil (unit: %); H_i is the thickness of each soil layer (unit: mm). In this experiment, the soil depth ranges from 0 to 100 cm and is divided into five layers (n = 5).

By adopting the water balance method, the water consumption in the experimental area can be calculated with the following equation:

$$\Delta W = W_i - W_j \quad (3)$$

$$ET = P + I + K - \Delta W - D - R \quad (4)$$

where ET is the water consumption in the experimental area (unit: mm); ΔW is the change in soil water storage capacity from 0 to 100 cm (unit: mm); P is the precipitation quantity; I is the irrigation water quantity (unit: mm); K is the groundwater recharge (unit: mm); D is the deep seepage water (unit: mm); R is surface runoff (unit: mm); W_i and W_j are the initial and final soil water storage capacity, respectively at a certain stage (unit: mm). Since there was no irrigation design in this experiment, I=0. The experimental area was surrounded by isolation belts (20 cm high), and as there

was no surface runoff during the experimental period, R=0. The precipitation in the experimental area was relatively low, and the soil layers were dry, which made it difficult for rainfall to fully penetrate the soil layers. Since most of the precipitation infiltration was stored in the soil layer, D can be negligible. Meanwhile, due to the deep burial depth of the groundwater in the experimental area, the groundwater recharge (K) can be negligible. Therefore, in this experiment, the main water input in the study area is precipitation (P), and the main output is water consumption (ET).

3 Results and discussion

3.1 Laboratory experiment

3.1.1 Soil infiltration process

The variation of soil infiltration rate over time for different treatment groups is shown in Fig. 4. Throughout the entire infiltration, the infiltration rate trends for different groups are similar, with a rapid decrease initially and then stability with time. Analyzing the changes in infiltration rates for different treatments (Tab. 3) indicates that the initial and average infiltration rates of ALS are significantly higher than those of NLS. The initial infiltration rates of ALS and NLS are 1.00 cm/min and 0.33 cm/min respectively, increasing by more than three times. The average infiltration rate of ALS is 67.57% higher than that of NLS. This is because a large number of macropores in the soil-rock mixed media of ALS during static air drying promote the formation of preferential flow [30], and these macropores are connected to the sandy soil in the sand ditches. During the infiltration, although the hydraulic conductivity of the soil-rock mixed media matrix area is small and can be negligible, these macropores can quickly infiltrate the water into the sand ditches with high hydraulic conductivity of the sandy soil. Thus, water can be rapidly stored from the upper soil layer and the infiltration water can be quickly supplied to the lower soil layer. Additionally, due to the soil expansibility, a large number of shrinkage cracks are generated during wetting expansion and drying shrinkage, which also enhances the soil infiltration capacity [31]. In the later infiltration stage, as the sand ditches may already be saturated with infiltrated water, the infiltration capacity is controlled by the lower soil layer. As a result, both ALS and NLS have the same infiltration capacity and similar stable infiltration rates.

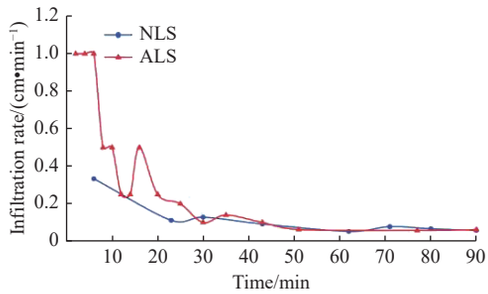

Fig. 4 Relationship between soil infiltration rate and time

Tab. 3 Soil infiltration rates of different treatments

treatment group	initial infiltration rate/ (cm·min^{-1})	steady infiltration rate/ (cm·min^{-1})	average infiltration rate/ (cm·min^{-1})
NLS	0.33	0.058	0.12
ALS	1.00	0.062	0.37

Considering the variation in cumulative soil infiltration volume (Fig. 5), the cumulative soil infiltration volume increases monotonically with time. Due to the faster initial infiltration rate of ALS, the cumulative infiltration volume shows a significant increase at the beginning, notably higher than that of the homogeneous NLS. However, as the infiltration time increases, the slope of cumulative infiltration volume levels off, bringing about a smaller increase in cumulative infiltration volume. At 90 minutes of the soil infiltration, the cumulative infiltration volumes of ALS and NLS are 16.8 cm and 8.88 cm respectively, indicating a 47.14% increase in the cumulative infiltration volume of ALS compared with NLS.

Gravel can facilitate the movement of soil moisture. Meanwhile, its significant bypass effect can extend the runoff path to hinder water movement. Both of the effects are mainly influenced by the gravel content [32]. In this experiment, the gravel volume ratio coefficient calculated from Equation (1) was 0.35, indicating that the hydraulic conductivity of the soil-rock mixed media was 0.55 times of the fine soil. This suggests that gravel in the soil reduces the infiltration capacity of the matrix area. This finding is consistent with the research of Wen et al. [33] and Ma et al. [34]. However, in the actual infiltration, the soil infiltration

capacity of ALS is much greater than that of NLS during the initial infiltration stage. In the later infiltration stage, the two are equivalent. The reason is that during the initial infiltration stage, the soil-rock mixed media generates a large number of cracks and macropores during static air drying, creating preferential flow and increasing hydraulic conductivity. In the later infiltration stage, as the fine soil in the lower layer determines the infiltration process, the infiltration capacity of ALS and NLS is the same.

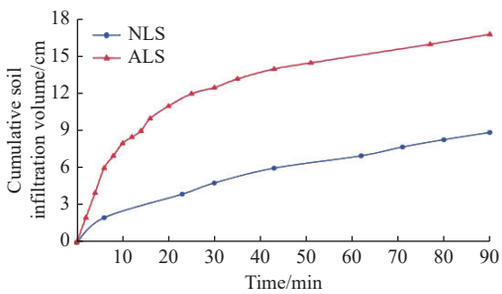

Fig. 5 Relationship between cumulative soil infiltration volume and time

3.1.2 Variation of soil water content

The variation of soil water content at different depths of the soil profile is shown in Fig. 6. The soil moisture at different layers follows a consistent dynamic pattern, gradually decreasing due to vegetation water consumption and soil evaporation, and sharply increasing after irrigation. Within the same time frame, in ALS treatment, the sandy soil layer has the lowest soil water content, with most of the time remaining below the soil capillary break water content (0.05 cm^3/cm^3). The soil water content in the surface layer at a depth of 0–10 cm is the second lowest, while the water content is the highest at a depth of 31–40 cm. In NLS treatment, the soil water content at different layers shows less variation. In comparison, the soil water content in the surface layer 0–10 cm of the ALS treatment is significantly lower than that of NLS. This is because, in the ALS treatment, gravel occupies a significant portion of the soil volume in the surface layer, reducing the water content. This is consistent with the findings of Han et al. [35], which state that gravel in fine soil will reduce the water content. The soil water profiles before and after irrigation (Fig. 7) showed that, after irrigation, the surface layer (0–10 cm) in the NLS treatment shows an increase in water content to 0.272 cm^3/cm^3, while the ALS treatment shows a water content of 0.221 cm^3/cm^3. In the deep layer (31–40 cm), the water content in the NLS treatment is only 0.277 cm^3/cm^3, while the ALS treatment reaches a high water content of 0.347 cm^3/cm^3. This indicates that ALS significantly improves the soil infiltration capacity to rapidly replenish the water content in the deep soil layer. In addition, the macropores and drying shrinkage cracks formed by the soil-rock mixed media facilitate rapid water infiltration, indirectly reducing the amount of downward infiltration water supply to the surface layer. In the sandy soil layer, except for the higher water content during and shortly after irrigation, the soil water content is below the residual water content (0.05 cm^3/cm^3) for most of the time. This is because the sandy soil has a low water holding capacity, and in the later irrigation stage, the film water in the sandy soil may be consumed through soil evaporation in the form of water vapor diffusion. In the 11–20 cm soil layer, the average water content is lower than that in the 21–30 cm layer. The reason is that the average soil water content of both layers is calculated by the area-weighted average method, and in the 11–20 cm layer, the weight of the sandy soil is relatively higher. Furthermore, Fig. 6 shows that compared with NLS, the ALS treatment shows a slower change in soil water content. This may be because the slower water consumption rate of evapotranspiration in ALS leads to slower water movement.

3.1.3 Soil evapotranspiration variation

Soil evapotranspiration includes vegetation transpiration and soil evaporation. In this study, the same-aged and same-sized spider plants were planted in the soil columns. Therefore, during the evapotranspiration calculation, the vegetation transpiration was considered the same, and the water consumption difference mainly originated from soil evaporation. The dynamic soil evapotranspiration in the vegetation water consumption experiment is shown in Fig. 8. Within the same time frame, the evapotranspiration of homogeneous NLS was significantly higher than that of ALS. During the observation period, the average daily evapotranspira-

tion of NLS was 4.35 mm, while that of ALS was 2.68 mm, which indicates that ALS can reduce ineffective soil evaporation by approximately 38.39%. The reason for this is as follows:

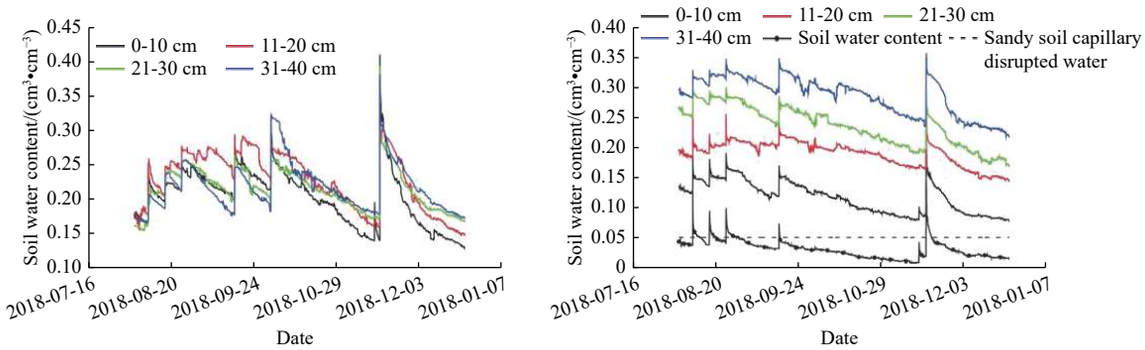

(a) No-artificially layered soil (NLS) (b) Artificially layered soil (ALS)

Fig. 6 Variation of soil water content over time

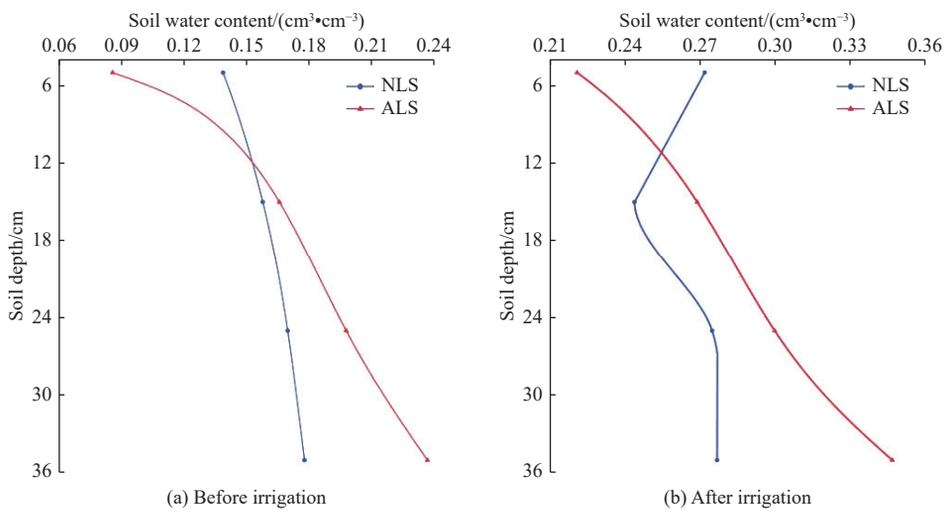

(a) Before irrigation (b) After irrigation

Fig. 7 Water content of soil profile before and after irrigation

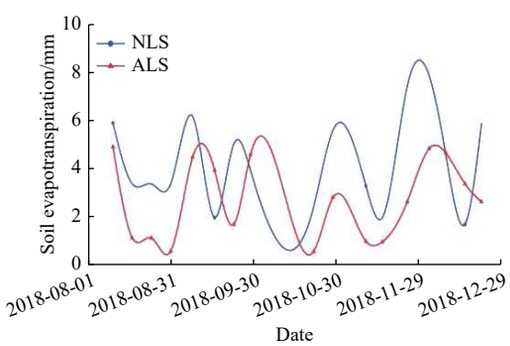

Fig. 8 Soil evapotranspiration variation over time

During soil evapotranspiration, a portion of the soil moisture is absorbed by plant roots and ultimately consumed through transpiration from the plant leaves. Another portion of the soil moisture moves from the wet area to the dry area under the action of capillary pressure, and it is consumed through soil evaporation at the soil surface. Numerous studies show that when the soil capillary connectivity is damaged, the liquid water movement essentially stops [36]. Liquid water in the soil can be divided into capillary water and film water. Generally, it is considered that film water exerts no significant impact on water movement and is often represented by the remaining (residual) water content [37]. Combined with Fig. 6(b), the water content in the sandy soil layer is lower than the remaining water content for most of the time. This indicates that during this period, the capillary water in the sandy soil layer is in a disrupted state, and the water in the deep soil layer can not be transported upward to replenish the surface soil through capillary water.

In the ASL treatment, the surface soil is mixed with a large amount of gravel, reducing the water holding capacity of the surface soil and the hydraulic conductivity of the matrix area to decrease soil

evaporation. Meanwhile, since the sandy soil layer blocks the capillary rise pathway, it is difficult for the surface soil to receive water supply from the deep soil, which causes prolonged dryness in the surface soil. Finally, ineffective soil evaporation is further reduced during evapotranspiration, which is consistent with the findings of Dong et al. [38].

In homogeneous NLS without gravel and sandy soil water-repellent layer on the surface, a portion of the water is consumed through vegetation transpiration during the non-irrigation period. Meanwhile, another portion of the water continuously moves from the deep soil to the soil surface under the action of capillary pressure. It is then consumed through ineffective soil evaporation, thereby increasing the ineffective soil evaporation and the total soil evaporation.

3.2 Field experiment

3.2.1 Time dynamics of soil water content

The variation of soil water content at different depths over time is shown in Fig. 9. Within the same time frame, the surface soil at a depth of 0–20 cm of the FUS control group has the highest soil water content, and the water content gradually decreases with the increasing soil depth. Compared with the control group, the ALS treatment group has the highest water content in the soil layer at a depth of 31–50 cm, and the surface soil at a depth of 0–10 cm has significant less water content than FUS. This may be due to a large amount of gravel in the surface soil of ALS, which occupies a considerable volume of soil to significantly reduce the soil water holding capacity [39]. Additionally, the sandy soil has a certain delaying and inhibiting effect on groundwater recharge, decreasing the water content in the upper soil layer of sandy soil [40-41]. Due to the strong hydraulic conductivity of the sandy soil, the soil water content at a depth of 31 –50 cm in ALS is significantly increased, which is consistent with the conclusion of Song et al. [42] that soil mixing with sand can significantly increase the soil water content below the mixing layer.

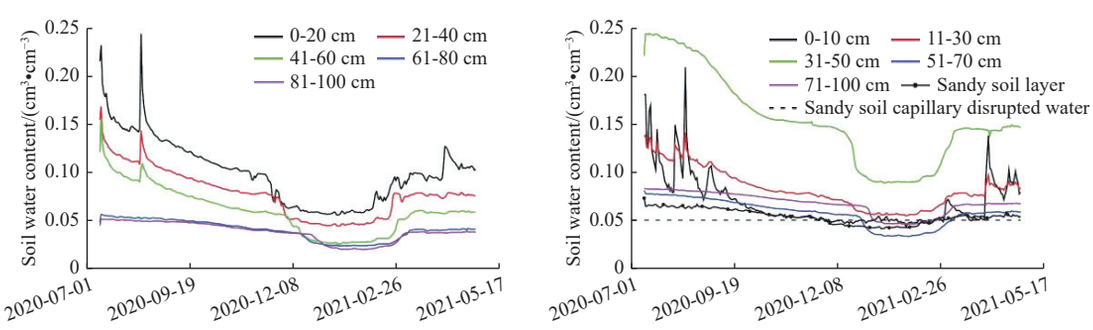

(a) Field undisturbed soil (FUS control group) (b) Artificially layered soil (ALS treatment group)

Fig. 9 Dynamic change of soil water content with time

3.2.2 Vertical change of soil water content

The vertical variation of soil water content (average values) for different treatments is shown in Fig. 10. In the FUS control group, the soil water content initially decreases with the increasing soil depth and then stabilizes. In the ALS treatment group, the soil water content shows a pattern of decrease-increase-decrease with the rising soil depth, eventually becoming stable. Combined with Fig. 9, the soil water content in the 0–30 cm depth range is higher in the FUS control group compared with ALS, while below 30 cm, the ALS soil has higher water content than FUS. Meanwhile, the FUS control group exhibits the highest soil water content in the surface layer, while the ALS treatment group shows the highest water content at a depth of 31–50 cm. This is because the formation of numerous drying shrinkage cracks and the presence of sandy soil in the soil-rock mixed media promote rapid water infiltration and improve the soil infiltration capacity. Additionally, the sandy soil can block capillary suction to maintain the surface soil in a dry state, and stores water in the lower soil

layer for plant utilization, thereby reducing ineffective soil evaporation.

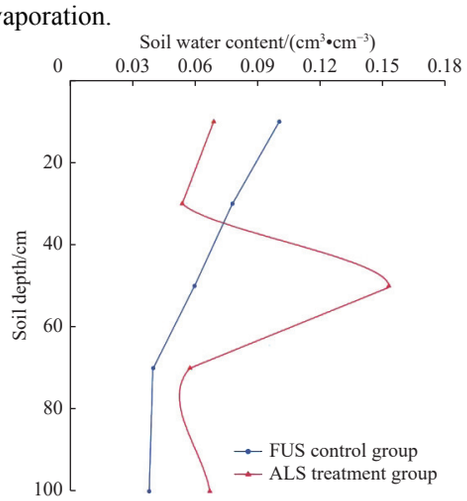

Fig. 10 Vertical changes of soil water content under different treatments

3.2.3 Water balance analysis

According to Equation (2), the soil water storage capacity can be calculated as shown in Fig. 11. The soil water storage capacity of different treatments fluctuates over time. In the FUS control group, the soil water storage capacity gradually decreases with increasing depth, and the water is mainly stored in the soil surface layer. In the ALS treatment group, the soil water storage capacity is mainly stored in the depth range of 31–50 cm below the surface.

According to Equations (3) and (4), the water consumption in the experimental area can be calculated for the period from July 2020 to October 2020, with the results shown in Tab. 4. The change in total soil water storage capacity for ALS is −38.78 mm, while it is −51.70 mm for FUS, approximately a 24.99% increase. Additionally, the water consumption for ALS is 84.08 mm, about 13.32% lower than that of FUS. In July and August, the water consumption rate of FUS is significantly higher than that of ALS. This is because there is more rainfall in July and August, and FUS stores most of its water in the surface soil, leading to higher evaporation. On the other hand, ALS promotes rapid water infiltration due to the presence of sandy soil and has capillary blocking effect, lowering soil water content in the surface layer and reducing ineffective soil evaporation. In September and October, due to climate changes, rainfall decreases sharply and ALS stores most of its water in deeper soil layers, which brings about lower ineffective evaporation, higher soil water content, and then higher water consumption rate. During the calculation period, the total water consumption rate for FUS is 0.93 mm/d, while it is 0.81 mm/d for ALS.

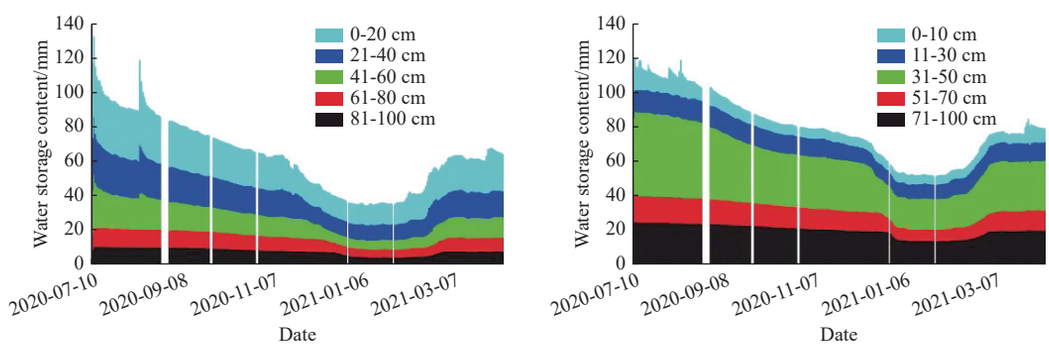

Fig. 11 Soil water storage capacity of different treatment methods

Tab. 4 Soil water balance with different treatment methods

date	rainfall/mm	FUS control group			ALS treatment group		
		change of soil water storage capacity/mm	water consumption capacity/mm	water consumption rate/(mm•d^{-1})	change of soil water storage capacity/mm	water consumption capacity/mm	water consumption rate/(mm•d^{-1})
2020-07	21.40	−25.41	46.81	2.23	−9.80	31.20	1.49
2020-08	20.90	−9.45	30.35	1.17	−5.88	26.78	1.03
2020-09	2.10	−8.53	10.63	0.38	−14.67	16.77	0.60
2020-10	0.90	−8.31	9.21	0.31	−8.43	9.33	0.32
total	45.30	−51.70	97.00	0.93	−38.78	84.08	0.81

4 Conclusions

The essence of ALS is to alter the original soil combination mode, enhance soil infiltration capacity, and influence soil water content by affecting water movement, thereby changing the distribution characteristics of the soil water. In this study, laboratory and field experiments were conducted through the ALS technique, and the following conclusions can be drawn.

In the infiltration ponding experiment, compared with the homogeneous NLS treatment, the initial infiltration rate of the ALS increases by more than three times, significantly accelerating the initial downward water movement. However, in the later infiltration stage, as the sandy soil layer reaches a saturated state, the soil infiltration capacity of the ALS and NLS treatments stabilizes and becomes similar. The average infiltration rate of ALS is 67.57% higher than that of NLS, and the cumulative soil infiltration volume is increased by 47.14%. In the ALS treatment, the sandy soil layer has the lowest water content, while the 30–40 cm soil layer has the highest water content. In homogeneous NLS, the water content is similar among different soil layers.

In the vegetation water consumption experiment, after implementing the ALS treatment, the water holding capacity of the surface soil decreases, and the sandy soil layer blocks the capillary rise pathway, reducing the ineffective soil evaporation by 38.39%.

In the field observation experiment, FUS has the highest water content in the soil layer at a depth of 0–20 cm, while ALS has the soil water content mainly stored at 31–50 cm below the surface, with significantly lower water content in the surface soil compared with FUS. The change in soil water storage capacity of the ALS treatment increases by 24.99% compared with FUS, and the water consumption decreases by 13.32%, with a significant reduction in the total water consumption rate.

The ALS technique is mainly employed for greening in extremely arid areas. The engineering construction is simple, and the required fine soil, gravel, and sandy soil are all natural available materials easy to obtain. Additionally, after ALS treatment, as long as the soil structure is not damaged, ALS can be adopted for a long time with just one treatment. Thus, it is highly valuable for large-scale promotion and application.

References:

[1] ZHAO J L, YANG Z Q, GOVERS G. Soil and water conservation measures reduce soil and water losses in China but not down to background levels: Evidence from erosion plot data[J]. Geoderma, 2019, 337: 729-741. DOI: 10.1016/j.geoderma.2018.10.023.

[2] LIU Y Q, WANG J L, LI Z Z. Research process on the effects of straw mulch on soil moisture and soil erosion[J]. Research of Soil and Water Conservation, 2021, 28(6): 429-436. DOI: 10.13869/j.cnki.rswc.2021.06.036.

[3] LIU C. Study on the effect of vegetation restoration on soil moisture on the Loess Plateau [D]. Shijiazhuang: Hebei University of Geosciences, 2022 (in Chinese).

[4] ZHAO R. Ecological adaptability evaluation and systematic development of desert restoration plants [D]. Tai 'an: Shandong Agricultural University, 2018 (in Chinese).

[5] ZOU H, GAO G Y, YUAN C A. Interactions between soil water and plant community during vegetation succession in the restored grasslands on the Loess Plateau of China[J]. Land Degradation & Development, 2022, 34(5): 1582-1592. DOI: 10.1002/LDR.4555.

[6] YANG K Y. Characteristics of photosynthesis and water use of *Caragana intermedia* plantation and related factors in Alpine sandy land [D]. Beijing: Chinese Academy of Forestry, 2019 (in Chinese).

[7] DU K, ZHANG B Y. Water characteristics of soil under different land-use types in Loess Hilly region[J]. Research of Soil and Water Conservation, 2020, 27(6): 72-76. DOI: 10.13869/j.cnki.rswc.2020.06.010.

[8] LI G L, WANG K, DUAN C H, et al. Study on simulation of soil water dynamics in fish-scale pit after rainfall in loess hilly region[J]. Research of Soil and Water Conservation, 2022, 29(2): 76-84, 91. DOI: 10.13869/j.cnki.rswc.20210630.002.

[9] XIE C J, WANG P, CHEN J. Effects of different mulching satterns on soil moisture, temperature and potato yield[J]. Chinese Journal of Soil Science, 2019,

50(5): 1151-1158. DOI: 10.19336/j.cnki.trtb.2019.05.20.

[10] LIU Y Q, ZHU X F, BAO X L, et al. Effects of the amount of corn straw mulching and returning to the field on the carbon metabolism activity and diversity of microorganisms in black soil[J]. Chinese Journal of Soil Science, 2023, 54(2): 407-415. DOI: 10.19336/j.cnki.trtb.2022101902.

[11] CHE Z, WANG J, LI J S. Effects of water quality, irrigation amount and nitrogen applied on soil salinity and cotton production under mulched drip irrigation in arid northwest China[J]. Agricultural Water Management, 2021, 247: 106738. DOI: 10.1016/j.agwat.2021.106738.

[12] GAN Y D, JIA Y W, QIU Y Q, et al. Stratified soil infiltration characteristics during rainfall[J]. Journal of Soil and Water Conservation, 2012, 26(5): 217-219,223. DOI: 10.13870/j.cnki.stbcxb.2012.05.027.

[13] GAN Y D, LI H, JIA Y W, et al. Infiltration-runoff model for layered soils considering air resistance and unsteady rainfall[J]. Hydrology Research, 2018, 50(2): 431-458. DOI: 10.2166/nh.2018.007.

[14] DENG C, SU Y, CAO Z C, et al. Study on the characteristics of different types of soil cracks[J]. Agriculture and Technology, 2022, 42(19): 90-93. DOI: 10.19754/j.nyyjs.20221015022.

[15] SI M F, GAN Y D, LIU H, et al. Effects of soil-rock mixed media gravel properties on soil infiltration and runoff process[J]. South-to-North Water Transfers and Water Science & Technology, 2018, 16(2): 59-63. DOI: 10.13476/j.cnki.nsbdqk.2018.0039.

[16] LI J M, SUN B, WANG Y F, et al. Differences in erosion and hydrodynamic characteristics of three kinds of residuals in mining area[J]. Journal of Yangtze River Scientific Research Institute, 2017, 34(10): 24-30. DOI: 10.11988/ckyyb.20160667.

[17] ZHAO M, WANG W L, GUO M M, et al. Erosion of slopes of lou soil stacks different in gravel content[J]. Acta Pedologica Sinica, 2020, 57(5): 1166-1176. DOI: 10.11766/trxb201905220129.

[18] GAN F L, HE B H, WANG T. Study on the characteristics of rainfall infiltration runoff using artificial simulation experiment in Wenchuan Earthquake Area[J]. Journal of Hydraulic Engineering, 2016, 47(6): 780-788. DOI: 10.13243/j.cnki.slxb.20150927.

[19] YOU J, WANG S Q. Impacts of soil fracture on cropland soil preferential flow and its controlling factors[J]. Water Saving Irrigation, 2022(9): 71-75,80.

[20] LYU W C, QIU Y, XIE Z K, et al. Effects of mulch gravel with different sizes on the process of water infiltration[J]. Research of Water and Soil Conservation, 2021, 28(6): 46-51. DOI: 10.13869/j.cnki.rswc.2021.06.004.

[21] ZHOU B B, SHAO M G. Effect of content and size of rock detritus on infiltration[J]. Acta Pedologica Sinica, 2007(5): 801-807. DOI: 10.3321/j.issn:0564-3929.2007.05.005.

[22] SHAO L Y, GAN Y D, SU H D, et al. The soil swelling on effects of rainfall infiltration tests[J]. China Rural Water and Hydropower, 2018, 11: 42-54. DOI: 10.3969/j.issn.1007-2284.2018.11.009.

[23] COPPOLA A, COMEGNA A, DRAGONETTI G, et al. Simulated preferential water flow and solute transport in shrinking soils[J]. Vadose Zone Journal, 2015, 14(9): 1-22. DOI: 10.2136/vzj2015.02.0021.

[24] COPPOLA A, GERKE H H, COMEGNA A, et al. Dual-permeability model for flow in shrinking soil with dominant horizontal deformation[J]. Water Resources Research, 2012, 48(8): W08527. DOI: 10.1029/2011WR011376.

[25] GAN Y D, LIU H, JIA Y W, et al. Swelling soil saturated water movement parameters calculating models[J]. Advanced Engineering Sciences, 2018, 50(2): 77-83. DOI: 10.15961/j.jsuese.201700680.

[26] WANG S S, ZHAI S X, FU Y L, et al. Study on the variation characteristics of rising capillary water of layered soil under variation of sand layer and thickness conditions[J]. Journal of Irrigation and Drainage, 2019, 38(11): 49-57. DOI: 10.13522/j.cnki.ggps.20190048.

[27] JIA Z J, LIU X Z, XU T Y, et al. Analysis of soil water evaporation characteristics and its influencing factor under mixed sand cover[J]. Journal of Soil and Water Conservation, 2023, 37(2): 227-236. DOI: 10.13870/j.cnki.stbcxb.2023.02.026.

[28] WANG Q J, WANG Z R, ZHANG J F, et al. Infiltration mechanism of layered soil and its simulation model[J]. Journal of Hydraulic Engineering, 1998(S1): 77-80. DOI: 10.13243/j.cnki.slxb.1998.s1.017.

[29] PECK A J, WATSON J D. Hydraulic conductivity and flow in non-uniform soil[C]. Workshop on Soil Physics and Field Heterogeneity, CSIRO Div. of Environmental Mechanics, Canberra, Australia, 1979:

31–39.

[30] SU H D, ZHAO S Y, JIA Y W, et al. Development path of preferential flow on soil-rock hillslope in the Chongling Watershed[J]. Journal of China Hydrology, 2019, 39(6): 1-6. DOI: 10.19797/j.cnki.1000-0852.20180304.

[31] WANG C, ZHANG Z Y, CHEN X A, et al. Dual-permeability model for crack preferential flow based on principle of water volume balance and its application[J]. Journal of Agricultural Machinery, 2021, 52(10): 314-326,348. DOI: 10.6041/j.issn.1000-1298.2021.10.033.

[32] FANG K, ZHENG J X, ZHANG L, et al. The influence of rock fragment cover on soil infiltration properties[J]. China Rural Water and Hydropower, 2020(2): 100-104. DOI: 10.3969/j.issn.1007-2284.2020.02.020.

[33] WEN M X. Experimental study on water movement of different soil-stone mixtures [D]. Yangling: Northwest Agriculture and Forestry University, 2011 (in Chinese).

[34] MA C L, LYU S H, PAN Y J, et al. Effect and sensitivity analysis of gravel parameterization on land surface process simulation in the Qinghai-Tibet Plateau[J]. Plateau Meteorology, 2020, 39(6): 1219-1231. DOI: 10.7522/j.issn.1000-0534.2020.00005.

[35] HAN C M, GAN Y D, JIA Y W, et al. Effects of the gravel physical properties of the soil-gravel media on water retention curve[J]. China Rural Water Conservancy and Hydropower, 2018(8): 86-90. DOI: 10.3969/j.issn.1007-2284.2018.08.018.

[36] SHAO M G, WANG Q J, HUANG M B. Soil Physics [M]. Beijing: Higher Education Press, 2006 (in Chinese).

[37] VAN GENUCHTEN M T, LEIJ F J, WU L. Characterization and measurement of the hydraulic properties of unsaturated porous media (parts 1 and 2) [C]// Proceedings of the International Workshop, Riverside, Calif. , 1997, 22–24.

[38] DONG R Z, YU M Y, QIU Z N, et al. A study on capillary water movement characteristics in sandy soil[J]. Water Saving Irrigation, 2018(4): 19-25. DOI: 10.3969/j.issn.1007-4929.2018.04.005.

[39] BOUWER H, RICE R C. Hydraulic properties of stony vadose zone[J]. Ground Water, 1984, 22(6): 696-705. DOI: 10.1111/j.1745-6584.1984.tb01438.x.

[40] JIA J C, ZHANG X C. Preliminary indoor simulation on water holding capacity of layered soils[J]. Research of Water and Soil Conservation, 2020, 27(6): 90-93,99. DOI: 10.13869/j.cnki.rswc.2020.06.013.

[41] CHEN S, MAO X M, BARRY D A, et al. Model of crop growth, water flow, and solute transport in layered soil[J]. Agricultural Water Management, 2019, 221: 160-174. DOI: 10.1016/j.agwat.2019.04.031.

[42] SONG R Q, CHU G X, YE J, et al. Effects of surface soil mixed with sand on water infiltration and evaporation in laboratory[J]. Transactions of the Chinese Society of Agricultural Engineering, 2010, 26(S1): 109-114.